Clays and Clay Minerals, Vol. 60, No. 5, 443–455, 2012.

MINERALOGICAL EVOLUTION OF A CLAYSTONE AFTER REACTION WITH IRON UNDER THERMAL GRADIENT

Marie-Camille Jodin-Caumon[1,*], Régine Mosser-Ruck[1], Aurélien Randi[1], Olivier Pierron[1], Michel Cathelineau[1], and Nicolas Michau[2]

[1] G2R, Université de Lorraine, CNRS, BP 70239, F-54506 Vandœuvre-lès-Nancy, France
[2] Agence nationale pour la gestion des déchets radioactifs (ANDRA), Direction Recherche et Développement/Service Colis et Matériaux, Parc de la Croix Blanche, 1/7 rue Jean Monnet, 92298 Châtenay-Malabry Cedex, France

Abstract—The design of the repository for high-level nuclear waste (HLW) in France consists of a multiple-barrier system including steel canisters in a clay host rock. The system will undergo temperature variations in time and space, the heat source being the HLW within the canisters. The effect of a thermal gradient in space on the Fe–claystone interaction was investigated here by applying a thermal gradient (150−300ºC and 80−150ºC) to a mix of claystone, Fe, and an aqueous chloride solution over periods of 3 and 6 months. Following the reaction, the starting clay minerals (mostly illite and mixed-layer illite-smectite) evolved toward chlorite, Fe-serpentine, Fe-saponite, mixed-layer chlorite-smectite, or mixed-layer serpentine-smectite as a function of temperature. Iron corrosion made the medium basic and reductive. Magnesium enrichment of clay minerals was observed in the hottest part of the experiment due to Mg migration under the thermal gradient. Reaction progress was enhanced at the lowest temperatures, compared to batch experiments.

Key Words—Crystal Chemistry, Iron, Mixed-layer Illite-smectite, Nuclear-waste Management, TEM-EDS, Thermal Gradient.

INTRODUCTION

Repositories located in deep geological formations are considered to be a possible solution for the long-term management of high-level nuclear waste (HLW). The concept developed in France, Japan, Switzerland, and Sweden consists of a multiple-barrier system including steel components (liner, canister, overpack, *etc*.) in contact with clay minerals (clay host rock or bentonite). The properties of the clay minerals or formation, in particular swelling, adsorption, or self sealing, may be affected by heat and radiation emissions from the HLW, corrosion of the Fe canister, and clay desaturation/resaturation. The possible mineralogical evolution of clays in contact with metallic Fe in experimental conditions that simulate those of a HLW repository were examined in the present study.

Many studies have been carried out at a constant temperature in the range 25−300ºC (*e.g.* Madsen, 1998; Guillaume *et al.*, 2003; Neaman *et al.*, 2003; Guillaume *et al.*, 2004; Lantenois *et al.*, 2005; Bildstein *et al.*, 2006; Charpentier *et al.*, 2006; Wilson *et al.*, 2006a, 2006b; de Combarieu *et al.*, 2007; Martin *et al.*, 2008; Perronnet *et al.*, 2008; Schlegel *et al.*, 2008; Osacký *et al.*, 2009; Jodin-Caumon *et al.*, 2010; Marty *et al.*, 2010; Osacký *et al.*, 2010; Savage *et al.*, 2010; Schlegel *et al.*, 2010; de Combarieu *et al.*, 2011), though the system undergoes a thermal gradient over time (first an increase then a progressive decrease in the temperature of the HLW as its activity decreases within a few 100 to a few 1000 years) and space (from the HLW to the host rock).

The presence of a thermal gradient may, through convection and diffusion processes, create mass-transport phenomena as a function of the nature of the chemical elements, gradient intensity, and temperature. The effect of a thermal gradient on the Fe-bentonite system has been described previously. MX80 bentonite was placed in contact with Fe (Jodin-Caumon *et al.*, 2010) at temperatures between 80ºC (or 100ºC) and 300ºC, using an experimental design similar to that of Vidal and colleagues (*e.g.* Vidal, 1997; Vidal and Durin, 1999; Vidal *et al.*, 2012). The starting montmorillonite of the MX80 bentonite evolved into Fe-rich products: at the lowest temperature ($\leqslant$100ºC), mainly a trioctahedral smectite; at the highest temperature (300ºC), Fe-chlorite. The redox conditions varied, more reduced conditions being found at the highest temperatures. The migration of Mg toward the hottest point was also observed clearly. In the batch experiments of Guillaume *et al.* (2003) at 300ºC, the clay sample farthest from the Fe plate was also Mg-enriched, with an Fe-for-Mg substitution at constant Fe+Mg content. The end-product was a trioctahedral Fe,Mg-chlorite. The migration of Mg toward the warmer region was also described by Plötze *et al.* (2007) and Olsson and Karnland (2011) in thermal-gradient experiments with bentonite but without Fe. Plötze *et al.* (2007) also noticed a small decrease in the interlayer charge in the warmer part of their experiment.

* E-mail address of corresponding author:
Marie-Camille.Caumon@univ-lorraine.fr
DOI: 10.1346/CCMN.2012.0600501

Although previous experiments were carried out on bentonite, which could constitute the disposal cell plug or the clay engineered barrier, the French design for radioactive waste disposal required an investigation of the direct contact between the steel canister and the clay host rock, composed of illite-smectite and illite-rich claystone. The main objective of the present study, therefore, was to describe the evolution of a claystone in contact with metallic Fe under a thermal gradient. The mineralogy of the altered claystone sample was studied using transmission electron microscopy-energy dispersive X-ray microanalysis (TEM-EDS) and X-ray diffraction (XRD) techniques.

MATERIALS AND METHODS

Reactants

The claystone sample came from the Callovo-Oxfordian formation of the Agence nationale pour la gestion des déchets radioactifs (ANDRA) underground research laboratory (Bure, Meuse-Haute-Marne, France) located in the eastern part of the Paris basin. The sample was taken from a borehole (FOR1118) in the Maximum Clay Zone (MCZ) (Gaucher *et al.*, 2004), which consisted mainly of a clay fraction (illite, mixed-layer illite-smectite R1, chlorite, and a small amount of kaolinite and muscovite), carbonates (calcite, dolomite, ankerite), quartz, feldspars, and pyrite (Figure 2).

Claystone was ground manually to 40 μm and stored in a glove box under Ar. Starting samples consisted of ground claystone alone or mixed with Fe powder (<50 μm, Riedel-de-Haën, Hanover, Germany, >99.5%), and an Fe plate (35−45 mg). The fluid was Milli-Q water (18.2 MΩ-cm) or a NaCl-$CaCl_2$ aqueous solution (0.0207 mol kg^{-1} NaCl and 0.0038 mol kg^{-1} $CaCl_2$ in Milli-Q water). The mass ratios between claystone powder, Fe powder, and fluid are shown in Table 1.

Tube-in-tube experiments

The experimental design was similar to that described by Jodin-Caumon *et al.* (2010). A mix of 50 mg claystone powder, Fe powder, and an Fe plate was placed in one 3 cm-long Pt capsule. Claystone powder alone was placed in another. The two Pt capsules were placed at opposite ends of an 18 cm-long Au tube. The capsules had been drilled (∅ 500 μm) to favor the migration of fluid and individual particles or small aggregates along the tube. The holes were small enough to limit the migration of large clay aggregates. The Au tube was filled with fluid, welded, loaded in a glove box under Ar (to limit the amount of O_2 in the reactor), and pinched every 3−4 cm to form five precipitation niches. Four experiments were carried out at a 150−300ºC thermal gradient and one further experiment at 80−150ºC. The thermal gradient was applied to the tube by placing it in an autoclave at a pressure of 150 bar, transmitted by a compressed fluid (Hydro Lubric 120 B 5% in water, Houghton S.A.S., Villefranche-sur-Saône, France). One extremity of the autoclave was placed in an oven and the other end in a sleeve filled with circulating cold water. The system was horizontal. The temperature calibration curve (Jodin-Caumon *et al.*, 2010) was linear. The four experiments carried out under the 150−300ºC thermal gradient were paired as follows: the Pt capsule containing the claystone powder, Fe powder, and Fe plate mixture was located either in the hottest part (HP) or the coldest part (CP) of the Au tube, to check the reversibility of the reactions (Table 1). At the end of the experiments, the autoclave was cooled quickly with water. The Au tube was quenched in liquid N_2 to freeze the liquid phase and avoid any particle movement following experimentation, then cut into five sections using cutting pliers or a precision knife and kept in a freezer until analyzed.

Sample labeling

The samples from the different sections were labeled using first the duration of the experiment and the position of the sample in the hottest part (HP) or coldest part (CP), then the mean temperature of the section, followed by Pt or Au, depending on whether the sample was located inside the Pt capsule (HP and CP) or on the Au tube walls (all along the tube, including the HP and

Table 1. Experimental conditions and mean temperature in each section of the five thermal gradient experiments.

Experiment	Position of Fe	Duration (months)	Fe/A	F/A	Fluid	– Mean temperature (ºC) in section no. – 1 (HP)	2	3	4	5 (CP)
3m-HP	HP	3	0.3	12	H_2O	305	265	230	185	150
3m-CP	CP	3	0.5	12	H_2O	305	265	225	190	150
6m-HP	HP	6	0.5	9	NaCl-$CaCl_2$	305	265	230	190	155
6m-CP	CP	6	0.5	10	NaCl-$CaCl_2$	300	260	220	185	145
L6m-HP	HP	6	0.3	9	NaCl-$CaCl_2$	155	135	120	105	85

Position of Fe: position of the Pt capsule containing the claystone and Fe mix in the hottest part (HP) or in the coldest part (CP) of the Au tube; Fe/A: mass ratio of Fe powder to claystone powder; F/A: mass ratio of fluid to claystone powder.

CP) (Table 1). The Pt capsules were in sections 1 and 5. As an example, the sample 3m-HP/305Pt is the result of the 3-month experiment (3m) with Fe in the hottest part (-HP) of the tube, and the particles were from the Pt capsule at 305ºC (/305Pt). A prefix L (for low) was added to samples from the experiment that ran at a lower thermal gradient (80−150ºC).

Batch experiments

Claystone powder, Fe (powder and plate), and fluid were mixed in an autoclave. The Fe powder to claystone powder mass ratio was 1, and the fluid to claystone mass ratio was 10. A Teflon-lined autoclave (capacity ~24 mL) was used for the experiment at 150ºC, and a Au-lined warm-seal autoclave (capacity ~18 mL) for the experiment at 300ºC. The Au-lined autoclave was mechanically sealed by a Au disc. The Teflon-lined autoclave was closed by bolting. Autoclaves were then heated to 150ºC and 300ºC in two ovens. The internal pressure was that of the liquid-vapor equilibrium pressure. The temperature was stable to within ±2ºC. After 3 months, the autoclaves were quenched to 25ºC and opened under an Ar atmosphere. The samples were also collected under an Ar atmosphere and centrifuged. The solid was dried under Ar flux at room temperature. The samples were stored under an Ar atmosphere until analyzed.

Sample analysis

Transmission electron microscopy (TEM). TEM photomicrographs, energy dispersive spectra, and electron diffraction patterns were obtained on dried powder samples dispersed in ethanol and deposited on a micro grid (Formvar/Carbon 300 Mesh Ni, Agar Scientific, Essex, England). The Philips CM20 electron microscope was operated at 200 kV and was equipped with an ultra-thin-window X-ray detector. Microchemical analyses of isolated clay particles were obtained with an energy dispersive X-ray analyzer (EDAX) attached to the electron microscope. The analyses were carried out in nanoprobe mode, over 40 s, with a probe diameter of 10 μm. The K_{AB} factors were determined using standards, with a maximum error of 5% for each element. For each sample, 20 to 30 analyses were performed on isolated clay particles.

The relative proportions of Si, Al, Fe, Mg, Na, Ca, K, Ti, and S were measured in all samples. Only trace levels of Cl, Ti, and S were found. Structural formulae were calculated on the basis of 22 negative charges per half unit cell, *i.e.* an $O_{10}(OH)_2$ basis, and the elemental composition of the clay with respect to each element was reported in units of atoms per formula unit (a.p.f.u). The tetrahedral sheet was assumed to be filled with $(4-x)$ Si and xAl atoms (denoted ^{IV}Al). The octahedral sheet was composed of Fe, Mg, and the remaining Al (denoted ^{VI}Al). The possible octahedral and tetrahedral charge deficiencies were balanced by the interlayer cations Na and Ca and were expressed in equivalents per formula unit or equivalents per half unit cell (e.p.f.u.). Based on previous studies (Lantenois, 2003; Lantenois *et al.*, 2005; Rivard, 2011), Fe was not expected in the interlayer but only in the octahedral sheet. Iron in the starting clay minerals was 71% Fe^{3+} (Rivard, 2011). Using MX80 bentonite in similar experiments Guillaume (2002), Guillaume *et al.* (2003), and Jodin-Caumon *et al.* (2010) showed a variation in the oxidation state of Fe as a function of temperature and the presence or absence of an Fe plate. From Mössbauer analyses, the Fe was all Fe^{3+} without Fe plate, 75% Fe^{3+} in the coldest part with an Fe plate, and 40% Fe^{3+} at 300ºC with an Fe plate. Clearly the oxidation state of Fe varied along the Au tube. Determination of the Fe oxidation state in individual clay particles using electron energy loss spectroscopy (EELS), for example, was not possible because Fe becomes reduced by the electron beam (Calvert *et al.*, 2005). Here the oxidation state of Fe was not measured because the amount of product available was too small for Mössbauer spectroscopy analyses. The Fe was, therefore, assumed arbitrarily to be 100% Fe^{3+}. Consequently, the octahedral occupancy cannot be determined because this depends on the Fe oxidation state. Reference clay minerals (Kostov, 1968; Caillère *et al.*, 1982) were added to the diagrams to represent the poles of possible crystal-chemical modifications.

X-ray diffraction. The XRD data were recorded using two diffractometers. When the amount of product was small, the whole-rock XRD patterns on unoriented powder were recorded using a Zero Background Holder (Silicon holder) and a Philips X'pert Pro diffractometer with non-monochromatic CuKα radiation (λ1 = 1.54056 Å, λ2 = 1.54439 Å) equipped with an X'Celerator MPD detector. The operating conditions were 40 kV accelerating voltage, 40 mA tube current, step scanning at 0.017º2θ intervals, and 35 ms counting time per step. The pattern from the empty holder was subtracted. When the amount of product was sufficient, XRD patterns of oriented powders were also recorded from the fine-grained fraction (<2 μm) and after ethylene glycol (EG) vapor saturation at ambient temperature using a D8 Bruker diffractometer with CoKα1 radiation (λ = 1.7902 Å) and a LynxEye TM one-dimensional detector. The operating conditions were 35 kV accelerating voltage, 45 mA probe current, step scanning at 0.035º2θ intervals, and 3 s counting time. The background was subtracted. The powder was pressed down manually in the sample carrier to give the particles a slight preferential orientation. The diffractometer used was more sensitive at small angles, so the pattern given by the starting material was susceptible to variations, leading to different XRD patterns depending on which diffractometer was used. As few particles of product were present, XRD data could only be recorded from the samples inside the Pt capsules.

RESULTS

Effect of the thermal gradient range

The effect of the range of the thermal gradient on Fe−clay interactions was examined through a comparison of two samples of claystone mixed with Fe at ~150ºC for a period of 6 months. One sample was placed in the CP of a 145−300ºC experiment (sample 6m-CP/145Pt). The temperature gradient, Δ, was 155ºC. The second sample was in the HP of an 85−155ºC experiment (sample L6m-HP/155Pt). The temperature gradient, Δ, and temperature range of this sample were lower (Δ = 70ºC, temperature ⩽155ºC) (Table 1).

Crystal chemistry of the clay particles. The clay particles in sample 6m-CP/145Pt contained less Si (down to 2.2 a.p.f.u.) compared to the crystal chemistry of the claystone clay particles before the experiment (Figure 1). The Al, Mg, K, and Na+Ca contents also decreased, reaching zero in some particles. The sample was enriched in Fe (up to 3.2 a.p.f.u.). The most evolved clay particles were in the domain of Fe-chlorite or Fe-serpentine. The clay particles of sample L6m-HP/155Pt were clearly less evolved than those of sample 6m-CP/145Pt but the trend was similar: smaller Si and Al contents (down to 3 and 0 a.p.f.u., respectively), and greater Fe contents (up to 3 a.p.f.u.). The interlayer charge (I.C.) decreased to 0.05 e.p.f.u. in 6m-CP/145Pt, initially due to the loss of Na and Ca cations, but also K in some particles. The I.C. decreased to 0.28 e.p.f.u. in sample L6m-HP/155Pt, but no clear variations of K and Na+Ca were observed. The Mg content ranged between 0 a.p.f.u. and that of the starting mixed-layer illite-smectite (0.2 a.p.f.u. mean). The decrease in Mg was correlated with Fe enrichment. The most evolved clay particles were intermediate between mixed-layer illite-smectite and Fe-chlorite or Fe-serpentine.

XRD data. The XRD patterns of samples 6m-CP/145Pt and L6m-HP/155Pt were compared to that of the starting claystone (Figure 2). Only a few diffraction peaks were observed compared to initial clay. The accessory

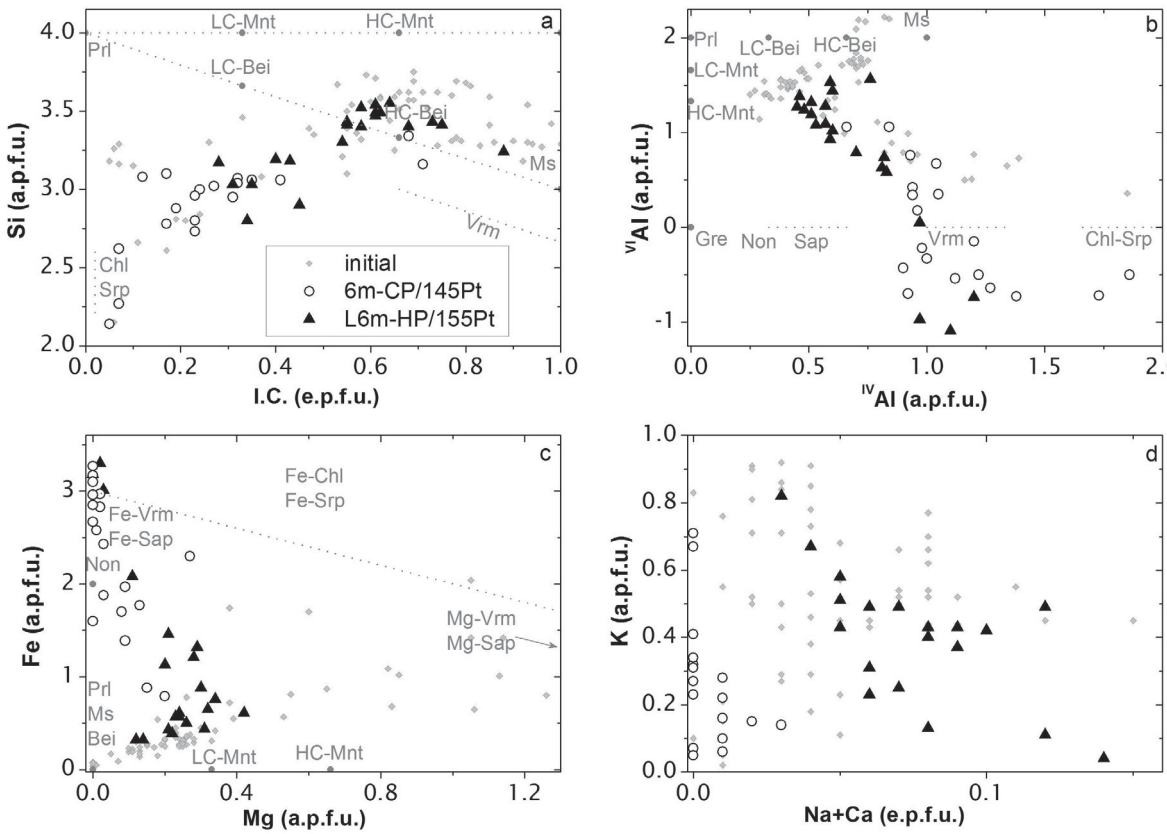

Figure 1. Crystal chemistry of samples 6m-CP/145Pt and L6m-HP/155Pt. (a) Si *vs* I.C.; (b) ^{VI}Al *vs.* ^{IV}Al; (c) Fe *vs.* Mg; (d) K *vs.* Na+Ca. Reference clays (Kostov, 1968; Caillère *et al.*, 1982) were Bei: beidellite; Chl: chlorite; Srp: 7 Å phases; Gre: greenalite; Mnt: montmorillonite; Ms: muscovite; Non: nontronite; Prl: pyrophyllite; Sap: saponite; Vrm: vermiculite; LC: low charge; HC: high charge; Al in octahedral sites $^{VI}Al = Al_{Tot} - {}^{IV}Al$ with $^{IV}Al = 4 - Si$.; interlayer charge, I.C. = Na + K + 2Ca. All structural formulae were calculated on the basis of the half unit cell, *i.e.* $O_{10}(OH)_2$. The axis units are atoms or equivalents per formula unit (a.p.f.u. or e.p.f.u., respectively) or per half unit cell.

minerals (carbonates, quartz, pyrite, and feldspars) were partially or totally dissolved. The clay minerals remained, as did some quartz and calcite, in sample L6m-HP/155Pt (Figure 2a). Magnetite was observed in

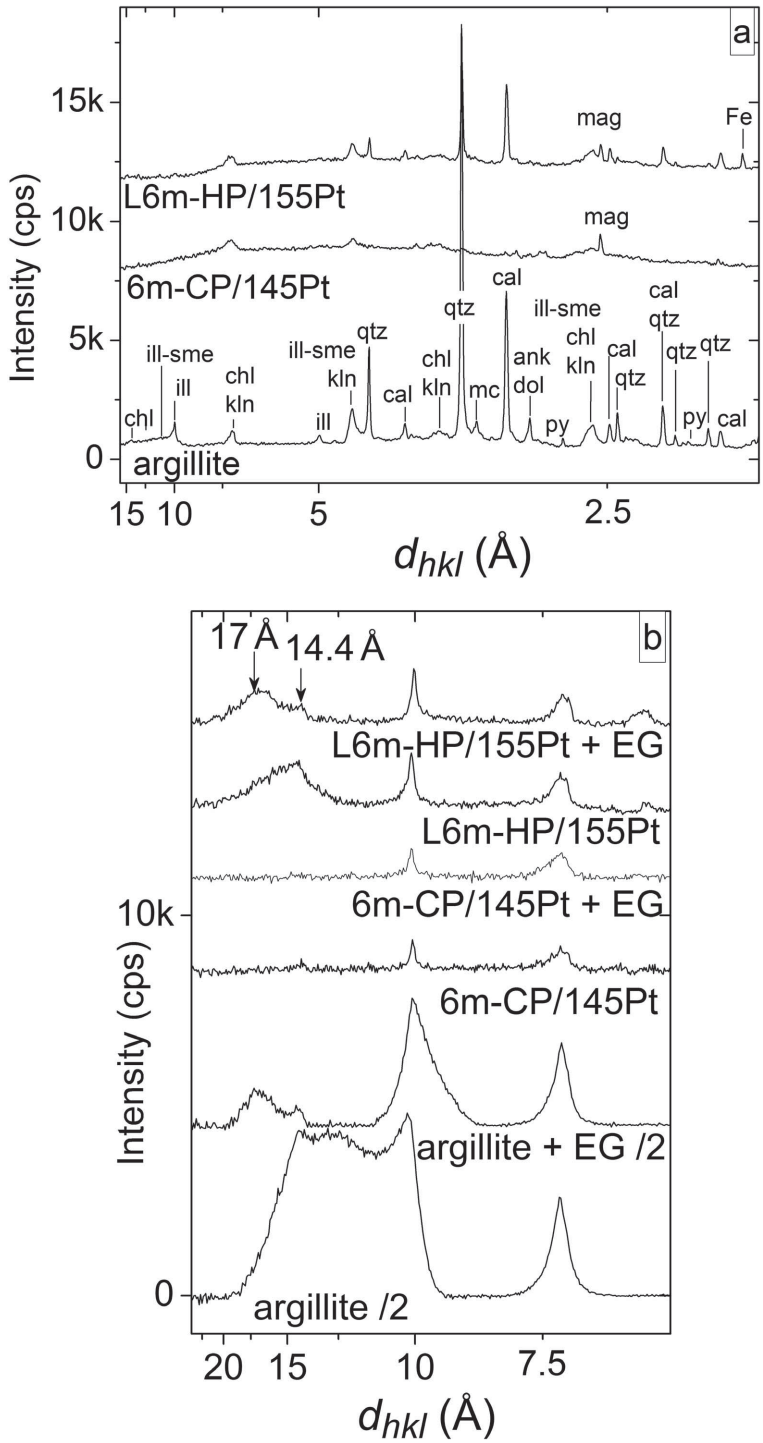

Figure 2. (a) XRD patterns of samples 6m-CP/145Pt and L6m-HP/155Pt compared to starting claystone. The XRD patterns are shifted along the vertical axis for the purposes of clarity. (b) XRD patterns of the air-dried fine fraction of starting argillite (divided by 2), and of samples 6m-CP/145Pt and sample L6m-HP/155Pt before and after EG vapor saturation. The XRD patterns are shifted along the vertical axis for the purposes of clarity. chl: chlorite; ill: illite; sme: smectite; kln: kaolinite; qtz: quartz; cal: calcite; mc: microcline; ank: ankerite; dol: dolomite; mag: magnetite; py: pyrite; Fe: metal iron.

both samples (main peak at 2.53 Å). Iron metal was still found in sample L6m-HP/155Pt (2.03 Å). In the fine-grained fraction, the amount of illite and mixed-layer illite-smectite decreased (Figure 2b), particularly in sample 6m-CP/145Pt, where only illite and 7 Å phases remained. A peak at 14.4 Å in sample L6m-HP/155Pt shifted partially to 17.0 Å after EG vapor saturation as in the starting material, attesting to the presence of the remaining illite-smectite or a new swelling clay mineral with a large Fe content such as Fe-saponite. A comparison with the crystal-chemistry data from TEM-EDS analyses suggested that the final reaction product in sample 6m-CP/155Pt was probably an Fe-serpentine. Sample L6m-HP/150Pt was less evolved and the least crystalline. The end products may be a mixed-layer Fe-serpentine-smectite (possibly with saponite as the smectite component). The mixed-layer phase might be an intermediary product between the starting mixed-layer illite-smectite and the final product of sample 6m-CP/150Pt, Fe-serpentine.

Comparison with batch experiments

Two samples from two experiments under the 150−300ºC thermal gradient (3m-HP/305Pt and 3m-CP/150Pt) were compared with two batch experiments run at the same temperatures (150ºC and 300ºC) (Figure 3). The Fe to claystone mass ratios were similar but the fluid to claystone mass ratios were higher in the batch experiments (*cf.* the section on Materials and Methods and Table 1).

At 300ºC. The crystal chemistry of the clay particles in sample 3m-HP/305Pt was very similar to that of the sample from the batch experiment at 300ºC (Figure 3). The Si, Al, and K contents and I.C. were smaller (down to 2.5, 0.55, 0.1 a.p.f.u., and 0.2 e.p.f.u., respectively). The Fe content increased (from 0.3 a.p.f.u. in the starting mixed-layer illite-smectite to 3.5 a.p.f.u.). The Mg content was about equal to that of the starting clay minerals (~0.2 a.p.f.u. for the mixed-layer illite-smectite). Some particles were enriched in Na+Ca in the batch sample. After reaction the clay particles were in a domain ranging from mixed-layer illite-smectite to Fe-chlorite or Fe-serpentine.

The structural evolution of both samples was also similar (Figure 4). The samples were poorly crystalline. Most of the minerals were dissolved, except calcite, Fe, and some clay minerals at ~7 Å and 14 Å (Figure 4a). A small peak of magnetite appeared (2.53 Å). The XRD analysis of the fine-grained fraction (Figure 4b) showed

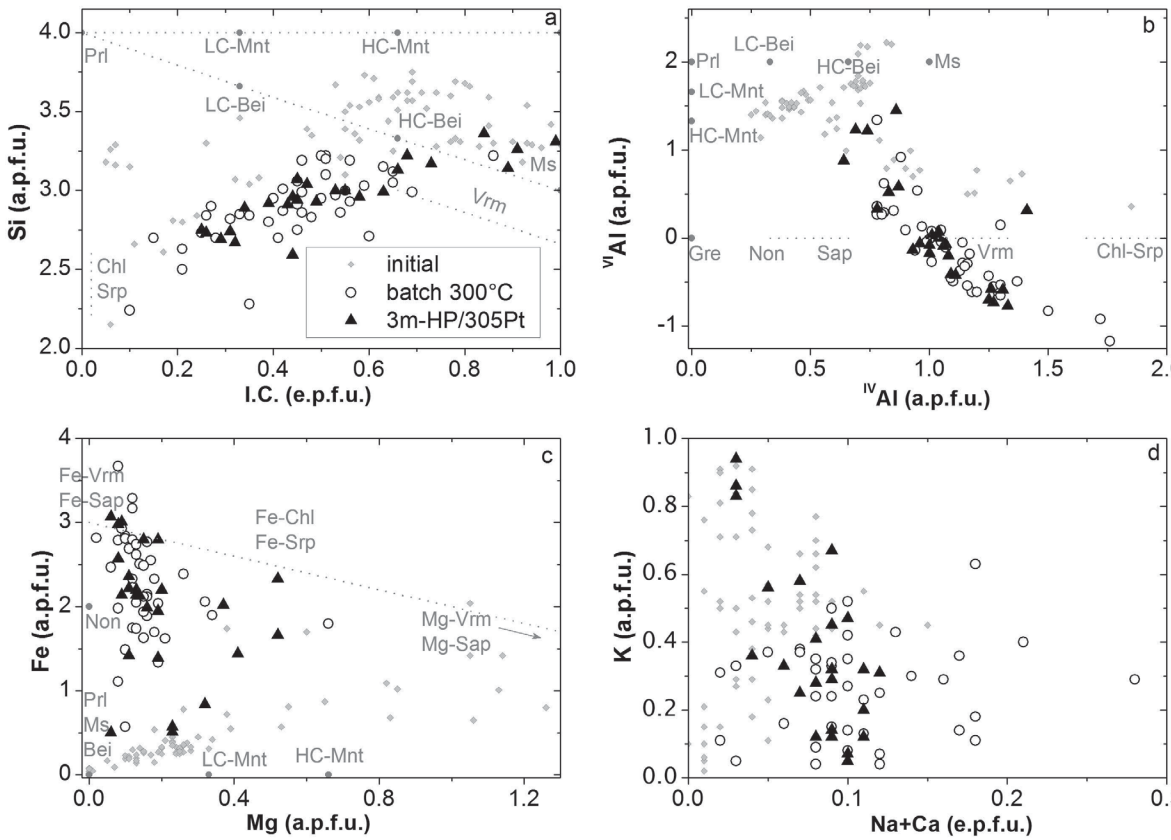

Figure 3. Crystal chemistry of sample 3m-HP/300Pt compared to the corresponding batch experiment at 300ºC. See Figure 1 for reference clays and axis units.

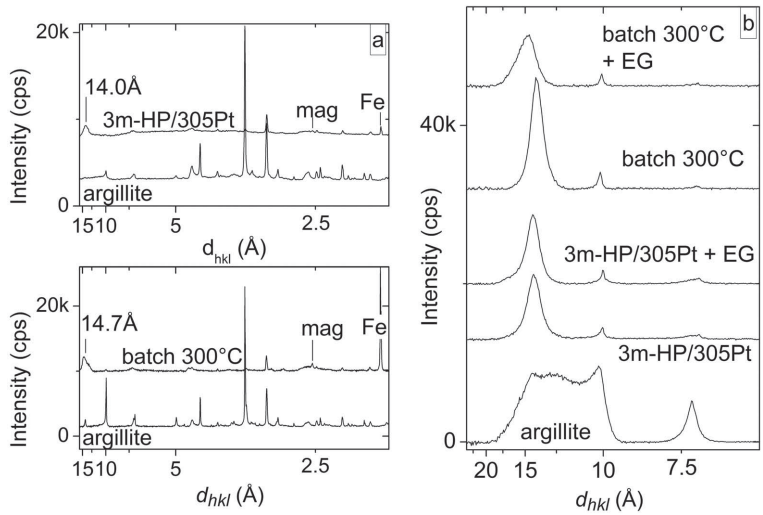

Figure 4. (a) XRD patterns of sample 3m-HP/305Pt (top) compared to the corresponding batch experiment at 300ºC (bottom) and starting claystone. Compare with Figure 2 for peak indexing. The XRD patterns are shifted along the vertical axis for the purposes of clarity. (b) XRD patterns of the air-dried fine fractions of starting argillite (or claystone), and of sample 3m-HP/305Pt compared to the corresponding batch experiment at 300ºC, before and after EG saturation. The lower-most XRD pattern was recorded in a configuration that favors small angles, which explains the differences in starting material. The XRD patterns are shifted along the vertical axis for the purposes of clarity.

a marked decrease in illite and of the phases with a peak at 7 Å (chlorite, serpentine, and/or kaolinite). The mixed-layer illite-smectite disappeared. Only swelling clays remained (peak at 14 Å broadening to 17 Å after EG saturation), in particular in the batch experiment; this could be smectite or saponite.

At 150ºC. The crystal chemistry of sample 3m-CP/150Pt was compared to the corresponding batch experiment run at 150ºC (Figure 5). The two samples showed similar trends but the sample under thermal gradient was, on average, more evolved. The clay had smaller Si, Al, and K contents, and less I.C. compared to the starting material (down to 3, 0, 0.05, and 0.1 a.p.f.u., respectively). The Na+Ca content was similar to that of the starting claystone (between 0 and 0.15 e.p.f.u.). Sample 3m-CP/150Pt was more Fe-enriched than the batch sample (up to 3.2 *vs.* 2.8 a.p.f.u.). The Mg content decreased to zero in sample 3m-CP/150Pt but remained almost constant in the batch sample (~0.2 a.p.f.u.). After reaction, the clay particles ranged between the domains of illite-smectite and those of Fe-chlorite and Fe-serpentine.

From a structural point of view, the two samples were very poorly crystalline (Figure 6). Some traces of clay minerals, calcite, quartz, and Fe remained (Figure 6a). The XRD pattern of the fine-grained fraction was also very poorly crystalline (Figure 6b). Only two small peaks were observed at 10.0 Å and 7.2 Å. A small peak near 14.5 Å probably shifted toward 17 Å after EG vapor saturation of the batch sample, which would correspond to a small amount of illite-smectite or saponite remaining.

Along the thermal gradient

The crystal chemistry of the clay particles found in sections 1, 2, 4, and 5 of the experiment 6m-CP were compared as a function of temperature and location (on the Au tube walls or inside the Pt capsules) (Table 1, Figure 7). Section 3 was empty. In this experiment, Fe was in the coldest part of the tube. The clay particles found on the Au tube walls could have been either particles of starting claystone that had migrated along the tube by convection, or clay minerals which crystallized from dissolved species. Very few particles were found on the Au tube walls at the end of the experiments, which made only TEM-EDS analyses possible. The crystal chemistry of the samples is described below, from the HP to the CP.

Sample 6m-CP/300Pt, at the HP in the Pt capsule, was rather heterogeneous, with a crystal chemistry extending over a range between the starting clay minerals and Mg,Fe-chlorite or serpentine (Figure 7). The Mg content was particularly large (up to 1.6 a.p.f.u.) compared to the other samples.

The crystal chemical domain of sample 6m-CP/260Au (just below sample 6m-CP/300Pt in temperature but on the Au tube wall) was similar, but more homogeneous. On average, this sample seemed to be more evolved than 6m-CP/300Pt, with lower I.C. and Si content (down to 0.2 e.p.f.u. and 2 a.p.f.u., respectively). The Mg content ranged between 0.2 and 1 a.p.f.u., from that of the starting mixed-layer illite-smectite to sample 6m-CP/300Pt, at constant Fe+Mg content (~3 a.p.f.u.).

Sample 6m-CP/185Au was divided into two groups. One group was not very evolved, with a slight decrease in Si content (down to 3 a.p.f.u.on average) and a small

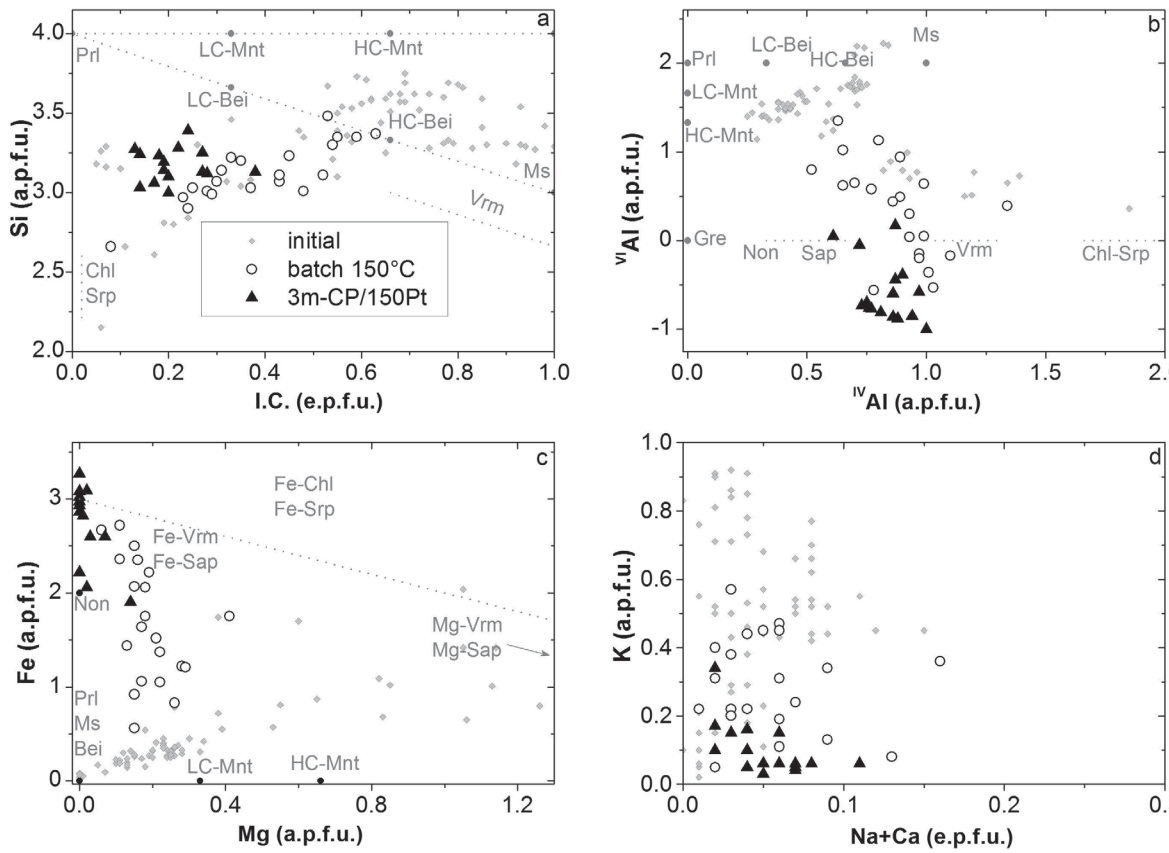

Figure 5. Crystal chemistry of sample 3m-CP/150Pt compared to the corresponding batch experiment at 150ºC. See Figure 1 for reference clays and axis units.

enrichment in Fe (up to 1.5 a.p.f.u.). The second group was similar to sample 6m-CP/260Au, except in Fe and Mg: this sample contained Fe only and no Mg.

Finally, sample 6m-CP/145Pt (at the lowest temperature and located inside the Pt capsule initially containing metallic Fe) was rather different from the others. The I.C. was relatively low (between 0.2 and 0.4 e.p.f.u.) but the Si content was average (around 3 a.p.f.u.). The Al and Na+Ca contents were very small, and the Fe content very large (up to 3.2 a.p.f.u.).

DISCUSSION

The state of Fe and the generation of the clay products and accessory minerals are summarized in Table 2.

Final clay products

Some samples were of very poor crystallinity, and the crystal chemistry properties of the reaction clay products were heterogeneous. The composition of the clay particles ranged widely, from the starting mixed-layer illite-smectite to an Fe-rich silicate, either serpentine or chlorite of similar composition. The formation of mixed-layer chlorite-smectite in similar experiments (at 250ºC), using high-resolution TEM imaging was reported by Wilson *et al.* (2006a, 2006b) and Jodin-Caumon *et al.* (2010). In the present work, the reaction products may also have been mixed-layer clay minerals. This might have corresponded to intermediary products between the starting material, mostly mixed-layer illite-smectite, and a final, stable product, chlorite or serpentine. As the space resolution of the TEM-EDS analysis was insufficient to analyze the layers individually, the chemical composition measured was the mean of the different mixed-layer phases.

At 300ºC, the end product seemed to be Fe-chlorite, or Fe-Mg-chlorite when Fe was at the other end of the tube, while at 150ºC, the reaction product was Fe-serpentine. The presence of serpentine at the lowest temperature and chlorite at 300ºC was consistent with the observation of Guillaume *et al.* (2003) and of natural assemblages: the maximum temperature of stability of a natural serpentine such as berthierine is 130ºC whereas chlorite is observed from 110 to 420ºC (Mosser-Ruck *et al.*, 2010 and references therein). The reaction products at intermediate temperature were more difficult to identify, as the quantity of particles found on the Au

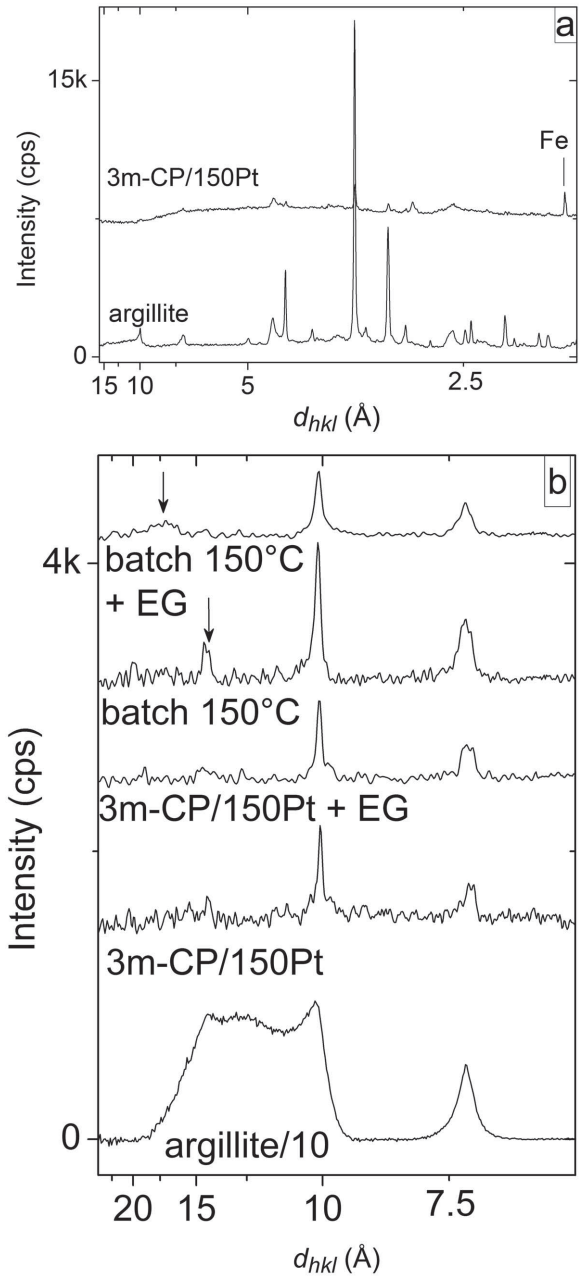

Figure 6. (a) XRD patterns of sample 3m-CP/150Pt (top) compared to the corresponding batch experiment at 150ºC (bottom) and starting claystone. Compare with Figure 2 for peak indexing. The XRD patterns are shifted along the vertical axis for the purposes of clarity. (b) XRD patterns of the air-dried fine fractions of starting argillite (divided by 10), and of sample 3m-CP/150Pt compared to the corresponding batch experiment at 150ºC, before and after EG saturation. The XRD patterns are shifted along the vertical axis for the purposes of clarity.

tube walls was very small. The observations at 185ºC (sample 6m-CP/185Au) showed that the sample was heterogeneous, with two groups of distinct chemical composition. The most evolved group was similar in composition to the products found at the highest temperature, except for Mg and Fe contents. A chemical discontinuity at ~180ºC was observed in similar experiments conducted on MX80 bentonite (Jodin-Caumon *et al.*, 2010), two different kinds of reaction progress pathways being observed in one sample. In the present work, although two different kinds of reaction progress were clearly observed, drawing any conclusions on reactive pathways was not possible, as one of the groups of particles exhibited only a very small evolution in comparison with the starting material.

Reaction progress

A comparison of samples found inside the Pt capsules in the thermal gradient experiments with the corresponding batch experiments (at 150 and 300ºC), and of different thermal gradients (150–300ºC *vs.* 80–150ºC) showed that the reaction kinetics at the CP were enhanced by the thermal gradient, but the reactive pathways were not modified. Processes in the CP were probably enhanced in the thermal gradient experiment by the presence of a connected medium at the highest temperature, acting as a sink for some elements such as Mg. The presence of reactive processes at higher temperatures may have shifted and modified equilibria in the coldest part of the tube.

A difference in reaction progress was observed between the samples from the Pt capsules and those found on the Au tube walls. One example is the comparison between samples 6m-CP/300Pt and 6m-CP/260Au. The sample at the lowest temperature, found on the Au tube walls, seemed to be more evolved than that at the highest temperature, located inside the Pt capsule. The difference in reaction progress was probably an effect of the fluid to claystone ratio: the volume of fluid in contact with the particles was clearly smaller inside the Pt capsules than in the intermediate sections. Reactivity may, therefore, have been enhanced outside the Pt capsules.

Migration of the elements

In experiment 6m-CP, metallic Fe was initially in the CP of the tube. The crystal chemical analysis of the clay end products clearly showed a strong enrichment in Fe and Mg in the samples at the highest temperature, attesting to the migration of Fe and Mg elements toward the HP of the tube. The Mg migration has already been observed in other studies run under a thermal gradient (Plötze *et al.*, 2007; Jodin-Caumon *et al.*, 2010; Olsson and Karnland, 2011; Vidal *et al.*, 2012) and in the batch experiments of Guillaume *et al.* (2003) as a function of the distance from the Fe plate. The behavior of other elements (Al, Si, K, Na, Ca) was more complex. The K content decreased in all samples, attesting to the dissolution of the illite fraction, in good agreement with the observations of de Combarieu *et al.* (2007). Using bentonite, Plötze *et al.* (2007) also observed a

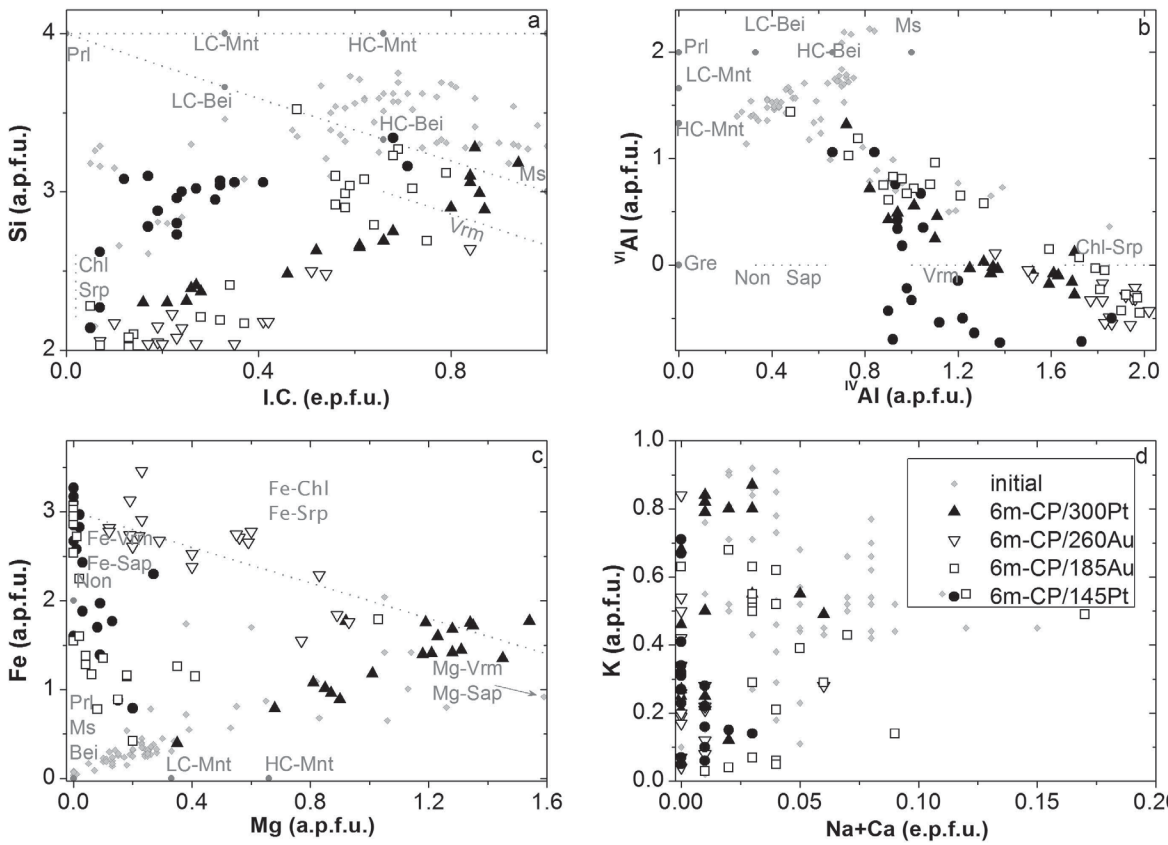

Figure 7. Crystal chemistry of samples 6m-CP/300Pt, 6m-CP/260Au, 6m-CP/185Au, and 6m-CP/145Pt. See Figure 1 for reference clays and axis units.

small decrease of I.C. near the heater. The evolution of Na+Ca content varied from one sample to another. As Na and Ca were present in the fluid at the beginning of the experiment, cationic exchange or surface sorption could not be excluded, and so no obvious correlation with mineralogical processes could be implied. In the samples initially mixed with metallic Fe, the Al content showed a marked decrease. At the same time, a decrease in the Si content in the clay minerals was observed, as was the dissolution of quartz in almost all of the samples. The generation of Al, Si, and K was not elucidated. They might have been present as dissolved species in the liquid phase, but the amount of fluid was so small that chemical analysis of the liquid was not possible. Dissolved species concentrations were measured in batch experiments using similar experimental conditions (de Combarieu *et al.*, 2007; Pierron, 2011; Rivard, 2011). Potassium and Si were present in significant amounts in fluids, but their concentrations were very dependent on physico-chemical conditions (pH, Eh, temperature, duration). De Combarieu *et al.* (2007) also suggested the formation of a gel prior to crystallization that could take up elements in its structure but such a gel was not observed in the present study .

Iron corrosion

Metallic Fe, initially present in the samples, oxidized to magnetite, which was the only Fe oxide observed. Iron corrosion generated hydroxide ions and H_2. As a consequence, the presence of Fe increased the pH and made the medium reductive. The pH increase was proven by the dissolution of quartz, which is greater in basic media, whereas calcite remained. The reductive conditions were consistent with the formation of magnetite. Pyrite was also reduced, which was attested to by the disappearance of the pyrite diffraction peaks on XRD patterns and by the odor of H_2S from some samples. The reaction product of the reduction of pyrite by H_2 might be pyrrhotite, as demonstrated by Truche (2009) and Truche *et al.* (2010), following the reaction: $FeS_2 + (1-x)H_2 = FeS_{1+x} + (1-x)\ H_2S$. However, the very small amount of pyrite in the claystone sample made detection of pyrrhotite impossible in the present study.

Comparison with MX80 bentonite

The effect of a thermal gradient on the Fe-bentonite system was described by Jodin-Caumon *et al.* (2010). The starting montmorillonite of the MX80 bentonite evolved into Fe-rich products similar to those observed in the

Table 2. Mineralogical composition of some samples at the end of the experiments.

Sample	Temperature (ºC)	Fe in sample[a]	Clay minerals[b]	Accessory minerals	Fe
Starting claystone			mixed-layer illite-smectite, illite, chlorite, kaolinite	quartz, calcite, dolomite, pyrite, felspars	
3m-CP/150Pt	150	yes	low crystallinity (Fe-serpentine?)	quartz, calcite	Metallic Fe
batch 150ºC	150	yes	low crystallinity (Fe-serpentine-smectite?)	calcite	magnetite, Metallic Fe
3m-HP/305Pt	305	yes	Fe-chlorite, mixed-layer illite-Fe-chlorite	calcite	magnetite, Metallic Fe
batch 300ºC	300	yes	Fe-chlorite, mixed-layer Fe-chlorite-smectite	calcite	magnetite, Metallic Fe
L6m-HP/155Pt	155	yes	mixed-layer Fe-serpentine-smectite (or saponite)	quartz, calcite	magnetite, Metallic Fe
6m-CP/145Pt	145	yes	Fe-serpentine	dissolved[c]	magnetite[c]
6m-CP/185Au	185	no	illite/Fe-serpentine products, Fe-chlorite or Fe-serpentine	No data	No data
6m-CP/260Au	260	no	Fe, Mg-chlorite	No data	No data
6m-CP/300Pt	300	no	Fe, Mg-chlorite	calcite, dolomite, pyrite[c]	$\varnothing^c$

[a]: Fe was mixed with the claystone powder (yes) or was in another part of the tube (no).
[b]: the most evolved clay products in the sample.
[c]: XRD data not shown.

present study: at the lowest temperature ($\leqslant$100ºC), mainly a trioctahedral smectite or a saponite and some Fe-serpentine; at the highest temperature (300ºC), Fe-chlorite. On the contrary, while quartz dissolution was observed here, amorphous silica products or newly formed quartz (depending on temperature) precipitated or crystallized in other experiments conducted with MX80 bentonite. The difference indicates differences in fluid composition during experiment, in particular pH and Si saturation level toward quartz, but these differences seem to have a weak effect on the final clay mineralogy. Chemical reactive pathways also appeared to be similar, with Fe corroding into magnetite, Mg migration toward HP, and the formation of mixed-layer chlorite-smectite, probably as intermediary products. The main difference concerned the amount of Fe-serpentine that was formed; the amounts formed were mostly greater when using argillite, possibly due to the presence of a larger amount of quartz in the starting sample, acting as a source of Si for serpentine crystallization.

CONCLUSIONS

These experiments identified two driving forces for enhancing fluid–mineral reaction: thermal gradient and Fe corrosion. Through these actions, the clay minerals were enriched in Fe, but depleted in Si, Al, and K. The I.C. decreased through the loss of the main interlayer cation K, which corresponded to the dissolution of illite. The clay minerals in the hottest part of the tube were also Mg-rich when Fe was in the coldest part. The clay particles at the end of the experiments were mostly mixed-layer phases, between the initial illite-smectite and an Fe-rich clay mineral. The end products were Fe-serpentine at 150ºC, with smectite, possibly an Fe-saponite in some cases due to large Fe contents, and Fe- or Fe,Mg-chlorite at 300ºC. However, the crystallinity of the end products was poor, particularly at the lowest temperatures (80–150ºC). Even if the reaction products at intermediate temperatures were not well determined, they were temperature dependent, reflecting the existence of local thermodynamic equilibria and discontinuous reactive pathways. Reaction progress at the CP was enhanced by the thermal gradient, but the reactive pathways did not appear to be modified. The presence of reactive processes at higher temperatures may have shifted and modified the equilibria in CP. Enhanced reaction progress was also observed in samples found on the Au tube walls compared to those found inside the Pt capsules, due to the effect of the fluid:claystone ratio. Whereas the starting mineralogy of the samples was different, and probably also fluid composition, the results are comparable to those obtained with MX80 bentonite (Jodin-Caumon *et al.*, 2010): Mg migration toward HP, reaction progress enhancement at CP, crystallization of magnetite, local thermodynamic equilibria, and final clay products. However, the amount of

Si available (provided by quartz dissolution in argillite) seems to be critical for the formation of Fe-serpentine at the lowest temperatures. Concerning HLW disposal repositories, the evolution of the starting illite-smectite toward serpentine or chlorite products would have consequences for the clay material or formation properties (swelling, adsorption, *etc*.) but the extent of the modifications induced cannot be predicted on the basis of the present results alone, due to significant differences between *in situ* conditions and laboratory experiments (especially temperature range, time, and fluid-to-solid ratio).

ACKNOWLEDGMENTS

This research was supported financially by ANDRA (the French National Agency for the Management of Radioactive Waste). The authors thank J. Ghanbaja (SCMEM, Université Henri Poincaré, Vandœuvre-lès-Nancy, France) for the TEM-EDS analyses and P. Villeger (LCSM, Université Henri Poincaré, Vandœuvre-lès-Nancy, France) for the XRD analyses using the Philips Xpert Pro diffractometer. U. Maeder and two anonymous reviewers are thanked for their useful and constructive comments. Associate Editor, R. Dohrmann is also thanked warmly for his careful reading of the manuscript which contributed much to the improvement of the quality of the manuscript.

REFERENCES

Bildstein, O., Trotignon, L., Perronnet, M., and Jullien, M. (2006) Modelling iron-clay interactions in deep geological disposal conditions. *Physics and Chemistry of the Earth, Parts A/B/C*, **31**, 618–625.

Caillère, S., Hénin, S., and Rautureau, M. (1982) *Minéralogie des Argiles. Structure et Propriétés Physico-Chimiques*. Masson, Paris, 184 pp.

Calvert, C.C., Brown, A., and Brydson, R. (2005) Determination of the local chemistry of iron in inorganic and organic materials. *Journal of Electron Spectroscopy and Related Phenomena*, **143**, 175–189.

Charpentier, D., Devineau, K., Mosser-Ruck, R., Cathelineau, M., and Villiéras, F. (2006) Bentonite–iron interactions under alkaline condition: An experimental approach. *Applied Clay Science*, **32**, 1–13.

de Combarieu, G., Barboux, P., and Minet, Y. (2007) Iron corrosion in Callovo-Oxfordian argilite: From experiments to thermodynamic/kinetic modelling. *Physics and Chemistry of the Earth*, **32**, 346–358.

de Combarieu, G., Schlegel, M.L., Neff, D., Foy, E., Vantelon, D., Barboux, P., and Gin, S. (2011) Glass-iron-clay interactions in a radioactive waste geological disposal: An integrated laboratory-scale experiment. *Applied Geochemistry*, **26**, 65–79.

Gaucher, E., Robelin, C., Matray, J.M., Négrel, G., Gros, Y., Heitz, J.F., Vinsot, A., Rebours, H., Cassagnabère, A., and Bouchet, A. (2004) ANDRA underground research laboratory: interpretation of the mineralogical and geochemical data acquired in the Callovian-Oxfordian formation by investigative drilling. *Physics and Chemistry of the Earth, Parts A/B/C*, **29**, 55–77.

Guillaume, D. (2002) Étude expérimentale du système fer – smectite en présence de solution à 80ºC et 300ºC. PhD thesis, Université Henri Poincaré, Nancy, France.

Guillaume, D., Neaman, A., Cathelineau, M., Mosser-Ruck, R., Peiffert, C., Abdelmoula, M., Dubessy, J., Villiéras, F., Baronnet, A., and Michau, N. (2003) Experimental synthesis of chlorite from smectite at 300ºC in the presence of metallic Fe. *Clay Minerals*, **38**, 281–302.

Guillaume, D., Neaman, A., Cathelineau, M., Mosser-Ruck, R., Peiffert, C., Abdelmoula, M., Dubessy, J., Villiéras, F., and Michau, N. (2004) Experimental study of the transformation of smectite at 80 and 300ºC in the presence of Fe oxides. *Clay Minerals*, **39**, 17–34.

Jodin-Caumon, M.-C., Mosser-Ruck, R., Rousset, D., Randi, A., Cathelineau, M., and Michau, N. (2010) Effect of a thermal gradient on iron-clay interactions. *Clays and Clay Minerals*, **58**, 667–681.

Kostov, I. (1968) *Mineralogy*. Oliver and Boyd, Edinburgh and London, 587 pp.

Lantenois, S. (2003) Réactivité fer métal/smectites en milieu hydraté à 80ºC. PhD thesis, Université d'Orléans, Orléans, France.

Lantenois, S., Lanson, B., Muller, F., Bauer, A., Jullien, M., and Plançon, A. (2005) Experimental study of smectite interaction with metal Fe at low temperature: 1. Smectite destabilization. *Clays and Clay Minerals*, **53**, 597–612.

Madsen, F.T. (1998) Clay mineralogical investigations related to nuclear waste disposal. *Clay Minerals*, **33**, 109–129.

Martin, F.A., Bataillon, C., and Schlegel, M.L. (2008) Corrosion of iron and low alloyed steel within a water saturated brick of clay under anaerobic deep geological disposal conditions: An integrated experiment. *Journal of Nuclear Materials*, **379**, 80–90.

Marty, N.C.M., Fritz, B., Clément, A., and Michau, N. (2010) Modelling the long term alteration of the engineered bentonite barrier in an underground radioactive waste repository. *Applied Clay Science*, **47**, 82–90.

Mosser-Ruck, R., Cathelineau, M., Guillaume, D., Charpentier, D., Rousset, D., Barres, O., and Michau, N. (2010) Effects of temperature, pH, and iron/clay and liquid/clay ratios on experimental conversion of dioctahedral smectite to berthierine, chlorite, vermiculite, or saponite. *Clays and Clay Minerals*, **58**, 280–291.

Neaman, A., Guillaume, D., Pelletier, M., and Villiéras, F. (2003) The evolution of textural properties of Na/Ca-bentonite following hydrothermal treatment at 80 and 300ºC in the presence of Fe and/or Fe oxides. *Clay Minerals*, **38**, 213–223.

Olsson, S. and Karnland, O. (2011) Mineralogical and chemical characteristics of the bentonite in the A2 test parcel of the LOT field experiments at Äspö HRL, Sweden. *Physics and Chemistry of the Earth, Parts A/B/C*, **36**, 1545–1553.

Osacký, M., Honty, M., Madejová, J., Bakas, T., and Šucha, V. (2009) Experimental interactions of Slovak bentonites with metallic iron. *Geologica Carpathica*, **60**, 535–543.

Osacký, M., Šucha, V., Czímerová, A., and Madejová, J. (2010) Reaction of smectites with iron in a nitrogen atmosphere at 75ºC. *Applied Clay Science*, **50**, 237–244.

Perronnet, M., Jullien, M., Villiéras, F., Raynal, J., Bonnin, D., and Bruno, G. (2008) Evidence of a critical content in Fe(0) on FoCa7 bentonite reactivity at 80ºC. *Applied Clay Science*, **38**, 187–202.

Pierron, O. (2011) Interactions eau-fer-argilite: Rôle des paramètres Liquide/Roche, Fer/Argilite, Température sur la nature des phases minérales. PhD Nancy Université – Université Henri Poincaré, Nancy, France.

Plötze, M., Kahr, G., Dohrmann, R., and Weber, H. (2007) Hydro-mechanical, geochemical and mineralogical characteristics of the bentonite buffer in a heater experiment: The HE-B project at the Mont Terri Rock Laboratory. *Physics and Chemistry of the Earth*, **32**, 730–740.

Rivard, C. (2011) Contribution à l'étude de la stabilité des minéraux constitutifs de l'argilite du Callovo-Oxfordien en

présence de fer à 90ºC. PhD thesis, Nancy-Université – INPL, Nancy, France.

Savage, D., Watson, C., Benbow, S., and Wilson, J. (2010) Modelling iron-bentonite interactions. *Applied Clay Science*, **47**, 91–98.

Schlegel, M.L., Bataillon, C., Benhamida, K., Blanc, C., Menut, D., and Lacour, J.-L. (2008) Metal corrosion and argillite transformation at the water-saturated, high-temperature iron-clay interface: A microscopic-scale study. *Applied Geochemistry*, **23**, 2619–2633.

Schlegel, M.L., Bataillon, C., Blanc, C., Prêt, D., and Eddy, F. (2010) Anodic activation of iron corrosion in clay media under water-saturated conditions at 90ºC: Characterization of the corrosion interface. *Environmental Science & Technology*, **44**, 1503–1508.

Truche, L. (2009) Transformations minéralogiques et géochimiques induites par la présence d'hydrogène dans un site de stockage de déchets radioactifs. PhD thesis, Université Toulouse III Paul Sabatier, Toulouse, France.

Truche, L., Berger, G., Destrigneville, C., Guillaume, D., and Giffaut, E. (2010) Kinetics of pyrite to pyrrhotite reduction by hydrogen in calcite buffered solutions between 90 and 180ºC: Implications for nuclear waste disposal. *Geochimica et Cosmochimica Acta*, **74**, 2894–2914.

Vidal, O. (1997) Experimental study of the thermal stability of pyrophyllite, paragonite, and clays in a thermal gradient. *European Journal of Mineralogy*, **9**, 123–140.

Vidal, O. and Durin, L. (1999) Aluminium mass transfer and diffusion in water at 400–550ºC, 2 kbar in the K_2O-Al_2O_3-SiO_2-H_2O system driven by a thermal gradient or by a variation of temperature with time. *Mineralogical Magazine*, **63**, 633–647.

Vidal, O., Baldeyrou, A., Beaufort, D., Fritz, B., Geoffroy, N., and Lanson, B. (2012) Experimental study of the stability and phase relations of clays at high temperature in a thermal gradient. *Clays and Clay Minerals*, **60**, 200–255.

Wilson, J., Cressey, G., Cressey, B., Cuadros, J., Ragnarsdottir, K.V., Savage, D. and Shibata, M. (2006a) The effect of iron on montmorillonite stability. (II) Experimental investigation. *Geochimica et Cosmochimica Acta*, **70**, 323–336.

Wilson, J., Savage, D., Cuadros, J., Shibata, M. and Ragnarsdottir, K.V. (2006b) The effect of iron on montmorillonite stability. (I) Background and thermodynamic considerations. *Geochimica et Cosmochimica Acta*, **70**, 306–322.

(*Received 1 March 2012; revised 3 October 2012; Ms. 657; AE: R. Dohrmann*)